Contactin 4, -5 and -6 differentially regulate neuritogenesis while they display identical PTPRG binding sites

Oriane Mercati[1,2,3], Anne Danckaert[4], Gwénaëlle André-Leroux[5], Marco Bellinzoni[5], Laura Gouder[1,2,3], Kazutada Watanabe[6], Yasushi Shimoda[6], Régis Grailhe[7], Fabrice de Chaumont[8], Thomas Bourgeron[1,2,3] and Isabelle Cloëz-Tayarani[1,2,3,*]

[1]Human Genetics and Cognitive Functions, Institut Pasteur, 75015 Paris, France
[2]CNRS URA 2182 'Genes, synapses and cognition', Institut Pasteur, 75015 Paris, France
[3]Université Paris Diderot, Sorbonne Paris Cité, Human Genetics and Cognitive Functions, 75013 Paris, France
[4]Plate-Forme d'Imagerie Dynamique, Imagopole, Institut Pasteur, 75015 Paris, France
[5]Unité de Microbiologie Structurale, Institut Pasteur and CNRS UMR 3528, 75015 Paris, France
[6]Department of Bioengineering, Nagaoka University of Technology, Nagaoka, Niigata 940-2188, Japan
[7]Neurodegeneration and Applied Microscopy, Institut Pasteur Korea, Geyonggi-do 463-400, South Korea
[8]Unité d'Analyse d'Images Quantitative, Institut Pasteur, 75015 Paris, France
*Author for correspondence (isabelle.cloez-tayarani@pasteur.fr)

Biology Open 2, 324–334
doi: 10.1242/bio.20133343
Received 12th October 2012
Accepted 28th November 2012

Summary

The neural cell-adhesion molecules contactin 4, contactin 5 and contactin 6 are involved in brain development, and disruptions in contactin genes may confer increased risk for autism spectrum disorders (ASD). We describe a co-culture of rat cortical neurons and HEK293 cells overexpressing and delivering the secreted forms of rat contactin 4–6. We quantified their effects on the length and branching of neurites. Contactin 4–6 effects were different depending on the contactin member and duration of co-culture. At 4 days in culture, contactin 4 and -6 increased the length of neurites, while contactin 5 increased the number of roots. Up to 8 days in culture, contactin 6 progressively increased the length of neurites while contactin 5 was more efficient on neurite branching. We studied the molecular sites of interaction between human contactin 4, -5 or -6 and the human Protein Tyrosine Phosphatase Receptor Gamma (PTPRG), a contactin partner, by modeling their 3D structures. As compared to contactin 4, we observed differences in the Ig2 and Ig3 domains of contactin 5 and -6 with the appearance of an omega loop that could adopt three distinct conformations. However, interactive residues between human contactin 4–6 and PTPRG were strictly conserved. We did not observe any differences in PTPRG binding on contactin 5 and -6 either. Our data suggest that the differential contactin effects on neurite outgrowth do not result from distinct interactions with PTPRG. A better understanding of the contactin cellular properties should help elucidate their roles in ASD.

Key words: Contactin, Rat primary cortical neurons, 3D modeling, Co-culture between HEK cells and primary neurons, Neurite outgrowth, Neurite quantification, Protein tyrosine phosphatase receptor gamma

Introduction

The development and maintenance of neuronal networks depend on the differentiation of neurons and on the outgrowth and branching of their axons and dendrites. These processes are under the control of recognition molecules that interact with each other and involve phosphorylation steps of downstream protein effectors. Among these recognition molecules, the immunoglobulin superfamily of neural cell-adhesion molecules (Ig-CAMs) directly participates in brain development mechanisms as well as in synapse maturation and plasticity (Stoeckli, 2004). Contactins are a subfamily of Ig-CAMs. They represent major molecules for neuronal development and formation of synaptic contacts. Indeed, their roles in neuritogenesis, fasciculation of neurons, axonal and dendritic targeting, fine tuning of synapse formation and synaptic plasticity have been demonstrated (Murai et al., 2002; Shimoda and Watanabe, 2009; Stoeckli, 2010). The contactin subfamily consists of six structurally related members: contactin 1 (F3 or F9 or contactin), contactin 2 (TAG-1), contactin 3 (BIG-1), contactin 4 (BIG-2), contactin 5 (NB-2) and contactin 6 (NB-3). All contactins are attached at the cell membrane via a glycosylphosphatidyl inositol (GPI) anchor and lack intracellular domains. These proteins share 40–60% identity with each other at the amino acid sequence level (Ogawa et al., 1996; Shimoda and Watanabe, 2009). The extracellular part contains six Ig-like repeats similar to the Ig constant domains, followed by four fibronectin type III domains located closer to the plasma membrane. Like other GPI-linked proteins, active contactins exist in both membrane-bound and soluble forms (Rougon et al., 1994; Peles et al., 1995; Ye et al., 2011).

In rodents, contactins (Cntns) are expressed mainly in the central and/or peripheral nervous systems where they display distinct and partially overlapping patterns. For Cntn2, expression starts early in development while for other Cntns, it occurs mainly after birth (Shimoda and Watanabe, 2009; Zuko et al., 2011). Important roles have emerged for Cntns in different aspects of brain development and function. For example, Cntn1 has been shown to contribute to oligodendrocyte maturation (Hu et al., 2003). Its expression in specialized domains of myelinated fibers underlines its role in myelination (Gollan et al., 2003; Salzer et al., 2008; Labasque and Faivre-Sarrailh, 2010). Other Cntns have been less studied. Cntn4 acts as an axon guidance molecule in the mouse olfactory neural circuitry where it controls the establishment of odor maps (Kaneko-Goto et al., 2008). Cntn5 contributes to the development of glutamatergic neurons in the rat auditory brainstem (Toyoshima et al., 2009a), while Cntn6 orientates the growth of apical dendrites of deep layer cortical pyramidal neurons (Ye et al., 2008) and controls the normal projection and branching of axons of the corticospinal tract during development (Huang et al., 2012).

Molecular signaling of contactins is related to their structure. They contract heterophilic interactions with signaling partners or may serve as ligand themselves. Identified partners include amyloid precursor protein (APP), Notch and other Ig-CAMs such as CHL1 of the L1 family (Shimoda and Watanabe, 2009). Because of their role in neuronal development, a link with tyrosine phosphatases can be expected since these enzymes are also involved in such processes (Ensslen-Craig and Brady-Kalnay, 2004). Accordingly, recent data indicate that Cntn4, -5 and -6 selectively interact with the protein tyrosine phosphatase receptor gamma (Ptprg) through its carbonic anhydrase (CA) domain (Bouyain and Watkins, 2010a). The X-ray structure of the murine complex between the first four immunoglobulin (Ig) domains of Cntn4 and the CA domain of Ptprg has been solved. The key residues involved in the molecular interactions have been identified in mouse, but not in human (Bouyain and Watkins, 2010a).

Genetic studies of neuropsychiatric disorders have sparked off new interests in human contactins (CNTNs) and contactin associated proteins (CNTNAPs) because of their involvement in diseases such as autism spectrum disorders (ASD) (Burbach and van der Zwaag, 2009). Genetic alterations including copy number variants (CNVs) for *CNTN*3 (Morrow et al., 2008) *CNTN*4 (Glessner et al., 2009; Roohi et al., 2009; Cottrell et al., 2011), *CNTN*5 and *CNTN*6 (Saus et al., 2010; van Daalen et al., 2011) have been reported in ASD patients. Several reports have also linked the *CNTNAP2* gene, encoding for contactin-associated protein-like 2 (CASPR2), with ASD (Alarcón et al., 2008; Bakkaloglu et al., 2008). CASPR2 is a binding partner of CNTN2, and interestingly enough, its absence in mice reproduces the core autism-related behavioral deficits (Peñagarikano et al., 2011). Disruption of *CNTN* genes could alter the growth, branching and targeting of axons and dendrites in the brain of ASD patients. This is in accordance with the postulation of the long-range underconnectivity theory (Belmonte and Bourgeron, 2006; Geschwind and Levitt, 2007). Understanding more precisely how CNTNs differentially operate in the developing human brain has therefore become an important issue. Cntns share the properties to increase neurite outgrowth *in vitro* as demonstrated by distinct studies and types of neurons using simple contrast microscopy and manual counting.

For this study, we cultured large populations of rat primary cortical neurons in the presence of human embryonic kidney (HEK) cells for the delivery of soluble Cntns and set up an innovative automated quantitative analysis, with possible applications for mutational screening of Ig-CAM molecules in disease. We then investigated the effects of rat Cntn4, Cntn5 and Cntn6 on different aspects of neurite outgrowth. We also analyzed the molecular interactions of human PTPRG and human CNTN4, CNTN5 and CNTN6 by generating the 3D structures of each complex, respectively, using homology modeling and protein docking calculations. Finally, we tested the binding of a fusion protein of PTPRG on Cntn5 and -6 overexpressed in HEK cells. Our results show different increasing effects of Cntn4, Cntn5 and Cntn6 on neurite outgrowth and branching. We also observed significant differences in the structure of human CNTN5 and CNTN6 as compared to CNTN4, located at the crucial Ig2–Ig3 domains, with no direct consequence on PTPRG binding.

Results

A co-culture system of rat primary cortical neurons with transfected HEK293 cells for the measurement of neurite outgrowth

Primary rat cortical neurons were cultured in the presence of HEK293 cells transfected with a plasmid vector containing the cDNA of rat *Cntn4*, *Cntn5* or *Cntn6*. The respective proteins are GPI-anchored cell-adhesion molecules, the schematic structure of which is depicted in Fig. 1A. In transfected HEK293 cells, Cntn4, -5 and -6 proteins were almost exclusively expressed at membrane levels as shown by immunofluorescence experiments (Fig. 1B). Among HEK293 cell populations, the efficiency of transfection was found to be of 50% for each Cntn and remained constant in independent experiments (data not shown). Semi-quantitative analysis of fluorescence in permeabilized HEK293 cells revealed no statistical difference between the cell surface membrane and intracellular expression among the Cntns. Fluorescence at the plasmalemma accounted for 66–70%, and cytoplasm for 30–34% of total labeling for Cntn4, -5 and -6 proteins (Fig. 1C). Co-cultures of transfected HEK293 and MAP2-stained neurons are illustrated in Fig. 1D. Based on our observations, most of the neurons were not in direct contact with other cells. We can therefore assume that neurons elongated randomly without favoring contacts with surrounding cells. To determine whether the amounts of secreted forms of Cntns were proportional to the number of HEK293 cells, we performed Western blot analysis on HEK293 cell extracts and aliquots of culture supernatants. Two cell densities were used (Fig. 1E). We observed a single band for Cntn4, -5 and -6, at 130 kDa, corresponding to the expected size of these proteins. Our data clearly indicate that the amounts of secreted forms of Cntn4, -5 and -6 were directly related to cell densities, and therefore to the amount of anchored Cntn proteins at the level of cell membranes (Fig. 1E). Since the number of HEK293 cells apposed on neurons was kept identical in all conditions, the secreted forms of Cntns remained constant among independent cultures as illustrated in Fig. 1F. No secreted Cntn could be detected when neurons were cultured alone (Fig. 1F). To evaluate the concentration of secreted Cntns when overexpressed by HEK293, we loaded increasing amounts (0.5 to 25 ng) of commercialized mouse recombinant Cntn6 (R&D Systems, ref. 5890-CN) on gels and performed a Western blot analysis. As expected, signals from the

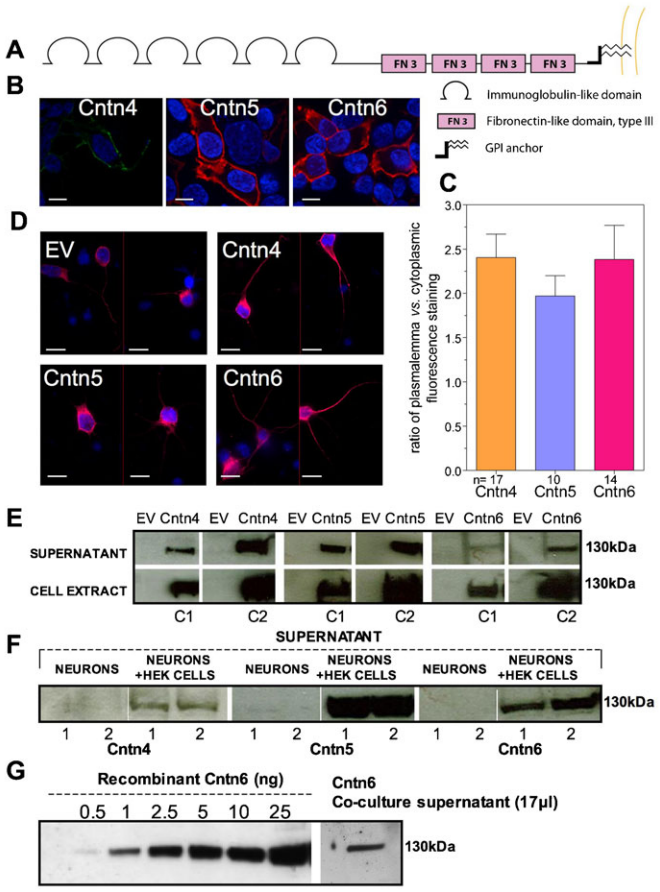

Fig. 1. Description of the co-culture system with analysis of secreted contactins. (**A**) Schematic structure of a contaction showing the six immunoglobulin-like domains and the four fibronectin-type III domains. The protein is attached to the membrane by a GPI moiety, and a soluble form is secreted upon GPI hydrolysis. (**B**) Membrane staining by immunofluorescence of non-permeabilized HEK293 cells after transfection with the *Cntn4*, *-5* or *-6* cDNA. Fixed cells were incubated with primary antibodies, then with Alexa 488-conjugated (Cntn4) and Alexa 594-conjugated (Cntn5 and -6) antibodies to Cntn as described in Materials and Methods. Scale bars=20 µm. (**C**) Semi-quantitative analysis of fluorescence in permeabilized HEK293 cells. Number of cells analyzed is indicated in the graphs. Values are the mean±s.e.m. Statistical analysis was performed using the Student's *t*-test. No significant difference was observed ($P>0.05$). (**D**) MAP2 staining of primary cortical neurons cultured in the presence of transfected HEK293 cells. In blue: DAPI nuclear staining. Some representative neurons are depicted in the absence and in the presence of Cntn4, Cntn5 or Cntn6. Note a higher ramification of neurons in the presence of Cntn5 as compared to Cntn4 and -6. Scale bars=20 µm. (**E**) Representative western blot of culture supernatants and HEK293 cell extracts for the detection of Cntn4, -5, and -6 proteins. Controls were obtained from HEK293 cells transfected with the empty vector (EV). Two cell densities (C1, C2) corresponding respectively to $\sim 1.5\times10^5$ and 3×10^5 cells were tested. (**F**) Representative western blot of co-culture supernatants. Rat cortical neurons were cultured in the presence of transfected HEK293 cells for 48–72 hours. No contactin proteins were detectable in the absence of HEK293 cells. Duplicates correspond to two independent co-cultures. (**G**) Western blot analysis of 0.5 to 25 ng of mouse Cntn6 and one aliquot of a co-culture supernatant for Cntn6. Exposure times were the same between all samples.

different amounts of Cntn6 were of increasing intensities (Fig. 1G). The signal intensity of the 17 µl-aliquot of a representative co-culture supernatant was close to the intensity of the 2.5 ng band. This suggests that under our experimental conditions, a concentration of Cntn4, -5 or -6 of at least 100 ng/ml could be raised and remains stable at least until 72 hours of co-culture (not shown).

Cntn4, -5 and -6 differentially increase the growth of rat primary cortical neurons

The automated quantification of neurite outgrowth was performed using the Acapella software as described in Materials and Methods. The sequential steps of analysis are depicted in Fig. 2. When primary neurons were co-cultured with HEK293 cells without Cntn expression, the length of the longest neurite and the numbers of roots and segments significantly increased between 4 and 6 days *in vitro* (DIV), and then they leveled off between 6 and 7–8 DIV (Fig. 3A). All neurons grew concomitantly in length and in branching as shown by plotting length *versus* roots and roots *versus* segments (Fig. 3B). In the latter graphs, slope values were calculated as an index of branching complexity. When neurons were co-cultured with HEK293 cells overexpressing the Cntns, increasing effects were observed on both neurite length and branching, but the effects were different depending on the Cntn member and duration of co-culture (Fig. 4A). At 4 DIV, Cntn4 and -6 significantly increased the length of the longest neurite, while Cntn5 increased the number of roots. All Cntns were increasing significantly the total number of segments per neuron. At 6 DIV, significant enhancing effects of Cntns were observed on the number of roots (Cntn4 and -6), on the length of the longest neurite (Cntn5 and -6), and on the total number of segments (Cntn5). At 7–8 DIV, slight increasing effects were observed for Cntn6 on the length of longest neurite and on the total number of segments. By contrast, Cntn4 and -5 did not display any significant effect on neurite elongation and branching. In the presence of Cntn4, -5 or -6, all neurons were growing concomitantly in length and branching as shown by plotting the number of roots *versus* the number of segments (supplementary material Fig. S1). Values for the Pearson's correlation coefficient and slope values were similar in all conditions between controls and Cntns (supplementary material Fig. S1).

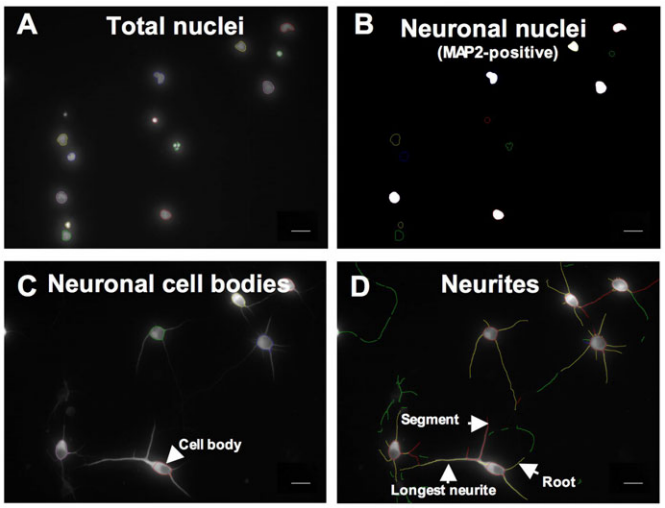

Fig. 2. Sequential automatic detection of neurite outgrowth and image processing by Acapella software (PerkinElmer). All cell nuclei are detected according to the DAPI staining (**A**). Neuronal nuclei are selected (**B**). Neuronal cell bodies are identified according to MAP2 staining (**C**). Neurites are identified and quantified (**D**). For quantification, all morphological parameters were measured under the same defined threshold conditions. Data are collected from at least 100 neurons. Neurons with no neurite were excluded. Scale bars = 20 µm.

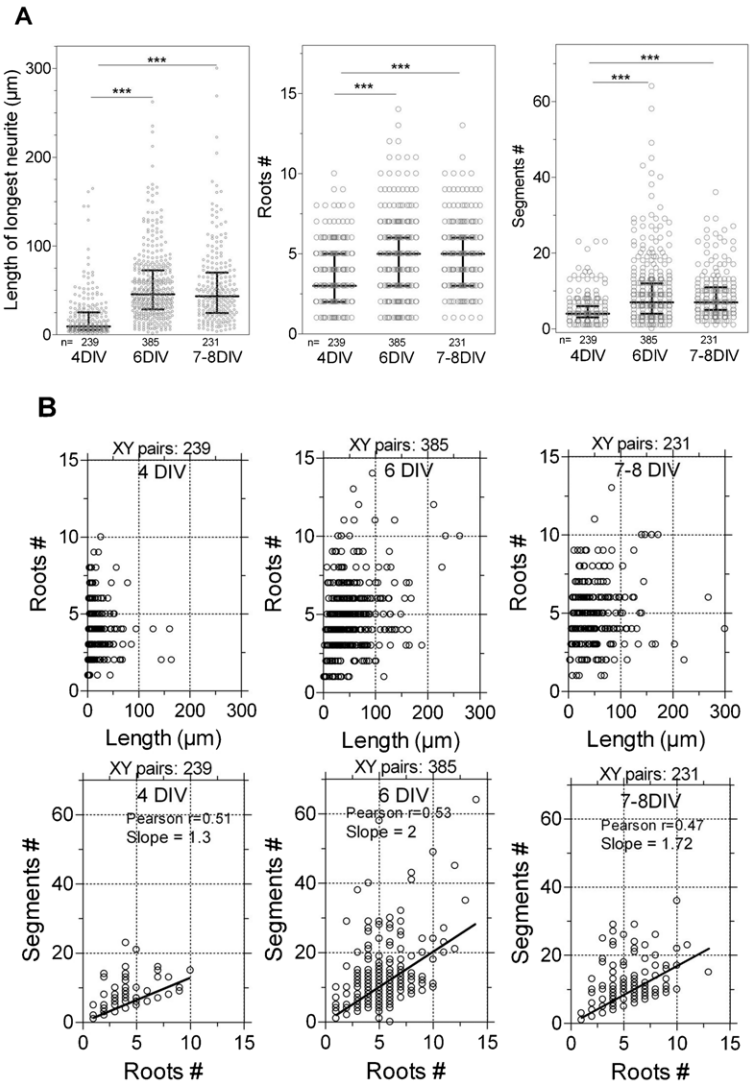

Fig. 3. Neurite outgrowth dynamics when cultured in the presence of HEK293 cells. Cultures of rat cortical neurons were established from newborn rats (P0–P1) as described in Materials and Methods. Neurons were kept for up to 8 days in culture (DIV). The same densities of HEK293 cells were added 48–72 hours before the end of culture, in all conditions (see Materials and Methods). The development of neuronal trees was followed over time. At the end of co-culture, neurons were fixed and immunostained with an anti-MAP2 antibody. (**A**) Quantification of neurite outgrowth parameters was performed using Acapella software. It includes the length of the longest neurite per neuron, the total number of roots, and the total number of segments. Graphs are scatter dot plots with a line at the median and the interquartile range. (**B**). Two-dimensional representations illustrating the evolution of neuronal trees over the different co-culture periods. Numbers of neurons analyzed are directly indicated in the graphs. The length of longest neurite *versus* number of roots and number of roots *versus* number of segments are represented. Slopes values and Pearson's correlation coefficients are indicated in the graphs. When primary neurons were co-cultured with HEK293 cells without Cntn expression, the length of the longest neurite, and the numbers of roots and segments increased significantly between 4 and 6 DIV and then leveled off between 6 and 7–8 DIV. Statistical analysis was performed using a Student's *t*-test. ***$P<0.001$.

Homology modeling of Ig domains 1–4 of human CNTN4, -5 and -6 and docking analysis of their respective interface with the CA domain of human PTPRG

The two-dimensional alignment of human CNTN4$^{Ig1–4}$, -5$^{Ig1–4}$ and -6$^{Ig1–4}$ with the homologous mouse Cntn4$^{Ig1–4}$ as a reference sequence is depicted in Fig. 5A. Models of human CNTN4$^{Ig1–4}$, -5$^{Ig1–4}$ and -6$^{Ig1–4}$ were obtained using the solved X-ray structure of the mouse Cntn4$^{Ig1–4}$ as 3D template (Fig. 5C). We observed an almost complete superimposition of the human CNTN4, -5 and -6 structures, except at one location for human CNTN5 and -6 as compared to mouse Cntn4 and human CNTN4. A loop with an omega shape was produced (Fig. 5C, middle and right panels). This was due to the insertion of two amino acid residues in human CNTN5 and -6 structures at positions V239 and V166, respectively (Fig. 5B). The conformational flexibility of the CNTN5 omega loop (Ω loop) was evidenced as the Ω loop clustered into three discrete positions, i.e. "up", "down" and "twist-up", among the 50 models generated. However, the "up" position appeared as a more stable conformational state when compared to the two other positions (Fig. 5C; supplementary material Movie 1). The carbonic anhydrase domain of human PTPRG (PTPRG^{CA}) was first modeled by using the mouse Ptprg^{CA} as a reference sequence and the 3D template of the complex of mouse Cntn4$^{Ig1–4}$/Ptprg^{CA} (Fig. 6A). Complexes between CNTN$^{Ig1–4}$ and PTPRG^{CA} appeared to be strongly stabilized through the alignment of β-sheet structures in both partners, in a close vicinity of the Ω loop (Fig. 6B). Each complex between human CNTN4, -5 and -6 and human PTPRG^{CA} was then modeled and optimized through energy minimization. A summary of the interface characteristics (surface of interaction, energy, hydrogen bonds and salt bridges) for each model is provided in Table 1. Contacts between Ptprg^{CA} and Cntn are restricted to Ig domains 2 and 3 and involve the same two discrete segments, including residues 129–142 in Ig2 and 220–228 in Ig3 (mouse Cntn4 (Bouyain and Watkins, 2010a)). Corresponding segments for human CNTNs were residues 130–141 in Ig2 and 220–250 in Ig3 (CNTN4), residues 203–215 in Ig2 and 295–325 in Ig3 (CNTN5) and residues 130–142 in Ig2 and 222–252 in Ig3 (CNTN6). The corresponding amino acids involved in the CNTN$^{Ig1–4}$/PTPRG^{CA} interaction were found to be strictly identical for CNTN4, -5 and -6 (Fig. 6C), strongly indicating an identical interaction of human CNTN4, -5 and -6 with PTPRG^{CA}.

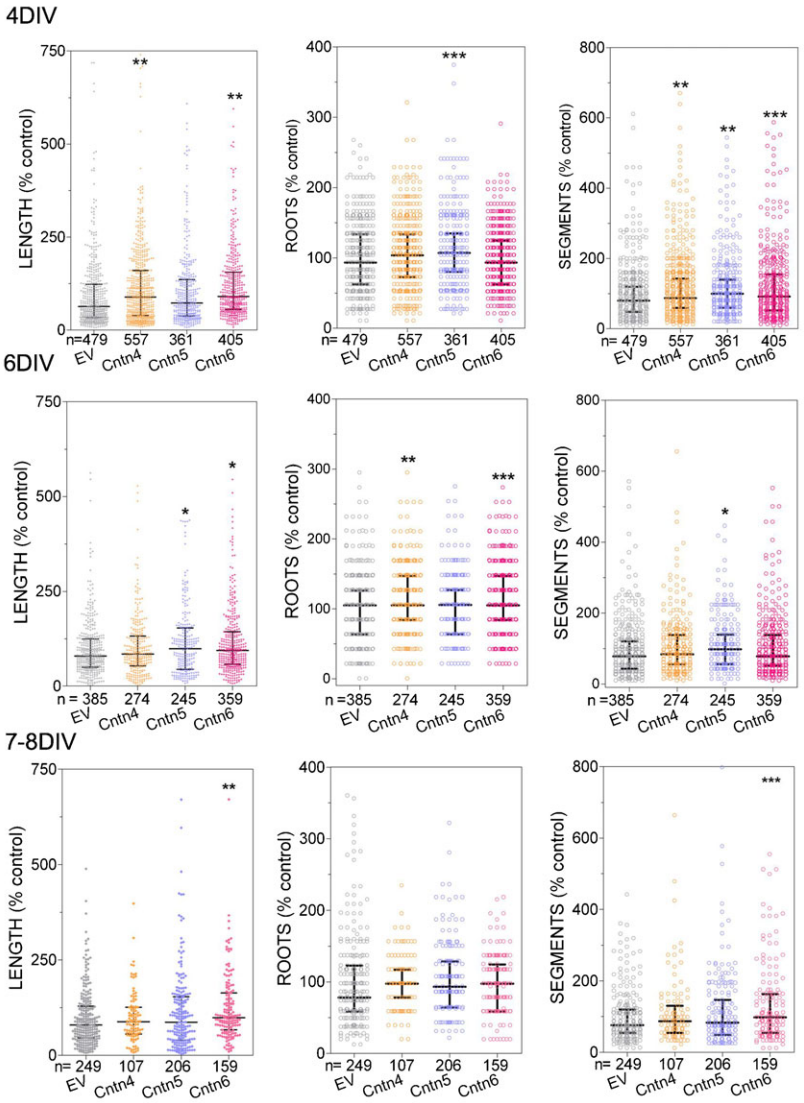

Fig. 4. Comparative effects of secreted Cntn4, -5, and -6 on neurite outgrowth in rat cortical neurons at different intervals of culture time. Cultures of rat cortical neurons were established from newborn rats (P0–P1) as described in Materials and Methods. Neurons were kept for up to 8 DIV. The same densities of HEK293 cells were added 48–72 hours before the end of culture, in all conditions (see Materials and Methods). The length of the longest neurite per neuron, the total numbers of roots and segments were followed over time in all conditions. At the end of culture, neurons were fixed and immunostained with an anti-MAP2 antibody. Quantification was performed using Acapella software. Numbers of neurons analyzed are indicated in each graph. Scatter dot plots with a line at the median and the interquartile range are represented. Data are expressed as percent of control mean obtained in the absence of Cntn. Statistical analysis was performed using a Student's *t*-test. $^{**}P<0.01$ and $^{***}P<0.001$. At early stages of growth, increasing effects of Cntn4 and -6 were pronounced on the length of the longest neurite (referred to as the length in graph abcissa). By contrast, increasing effects of Cntn5 were more pronounced on the number of roots and segments as an index of arborization.

Ptprg–Fc equally binds to the Cntn5 and Cntn6 over-expressed in HEK293 cells

In agreement with our modeling studies, we observed a significant binding of Ptprg–Fc to overexpressed rat Cntn5 and Cntn6 by HEK293 cells, as compared to HEK293 cells with no Cntn expression (Fig. 7A). Semi-quantitative analysis indicate that binding was of the same rank of order between Cntn5 and Cntn6 (Fig. 7B).

Discussion

Our study describes an efficient co-culture assay and an automated quantification method for the analysis of neurite outgrowth in cultured neurons and their morphological aspects including neurite length, and branching complexity, as a function of time. This assay provides an accurate analysis of a high number of cells allowing the detection of even subtle morphological variations in neurons. We applied this technique to analyze the effects of three members of the contactin family (Cntn4, -5, -6), a subgroup of cell-adhesion molecules that play essential roles in the development of neuronal circuits. We took advantage of the fact that contactins are GPI-anchored proteins, sorted into lipid rafts before transport to the membrane surface (Sharom and Lehto, 2002), and secreted into the extracellular matrix of cells. Their secretion is mediated by the activation of extracellular phosphoinositide-specific phospholipase C (PI-PLC), an enzyme that controls the surface expression and functional properties of GPI-anchored proteins (Ting and Pagano, 1991). Eight PI-PLC isoforms are expressed in HEK293 cells, and in the case of overexpression of a calcium sensor, an upregulation of one selective isoform, namely the PI-PLC-δ2 can be observed (Sharom and Lehto, 2002). Calcium signaling is therefore expected to control the PI-PLC activity and also the externalization of contactins as clearly demonstrated for the F3/contactin member (Pierre et al., 2001).

Neuritogenesis is a complex dynamic process combining neurite outgrowth and branching. Outgrowth results from the elongation and retraction of neurites with a concomitant rapid cytoskeleton reorganization at the growth cone (Valtorta and Leoni, 1999). In a first series of experiments, we followed the dynamics of neurite growth and branching, in the absence of Cntn, and at early stages of neuritogenesis. For this purpose, we used the exclusive labeling of dendritic trees of rat cortical

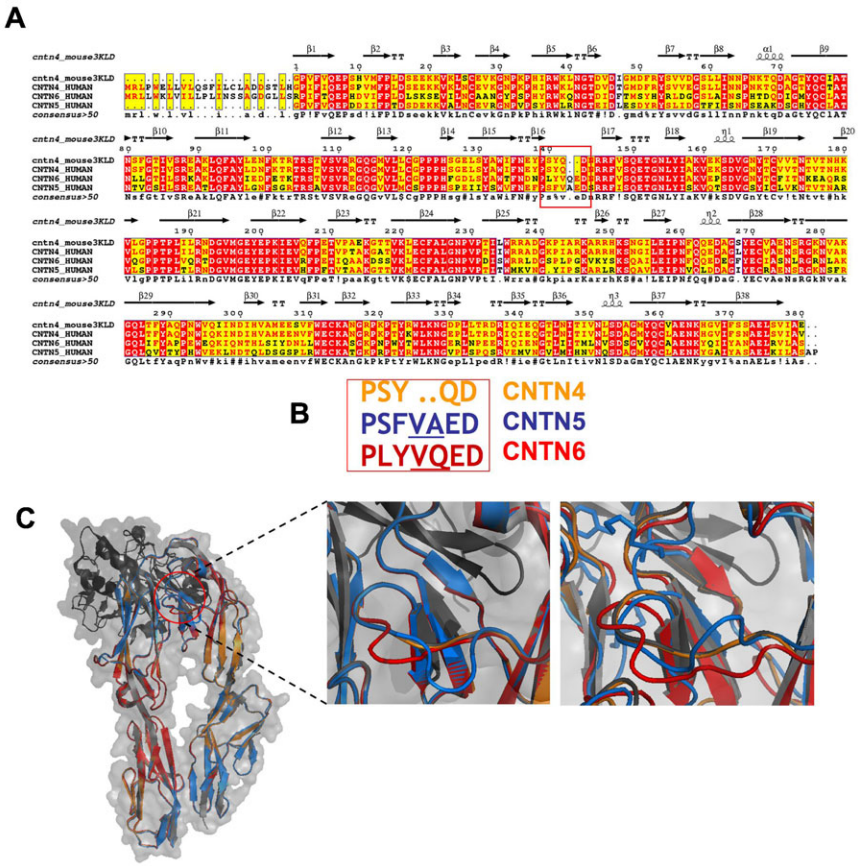

Fig. 5. Superimposed models of human CNTN4$^{Ig1–4}$, -5$^{Ig1–4}$, and -6$^{Ig1–4}$. (**A**) Two-dimensional alignment of human CNTN4$^{Ig1–4}$, CNTN5$^{Ig1–4}$, and CNTN6$^{Ig1–4}$ with the homologous mouse Cntn4$^{Ig1–4}$ (reference sequence: 3KLD FASTA and pdb). (**B**) Amino acid sequences in the Ω loop present at the Ig2–Ig3 interfaces in CNTN4, -5 and -6. An insertion of two amino acids is present in CNTN5$^{Ig1–4}$ and CNTN6$^{Ig1–4}$ as compared to CNTN4$^{Ig1–4}$. (**C**) Structures of CNTN4$^{Ig1–4}$ (in yellow), CNTN5$^{Ig1–4}$ (in blue) and CNTN6$^{Ig1–4}$ (in red) after homology modeling using the Cntn4$^{Ig1–4}$ as a template (Bouyain and Watkins, 2010a). Higher magnification of the Ω loop for CNTN5 with two structural positions (down in left panel and up in right panel). Structural images were generated using PyMOL (http://www.pymol.org).

neurons with an anti-MAP2 antibody. The extent of neurite outgrowth depends on the density of cells, and the constituents of culture medium including the growth factors. Therefore, to obtain reproducible results, the conditions under which the cells were grown were kept identical in all experiments. Neurons were co-cultured with HEK293 cells transfected with the empty vector with no Cntn expression. In these control conditions, a rapid growth and branching of neurites was observed until day 6 of culture, which slowed down thereafter. The growth amplitude, the number of branching points and the growth kinetics are in agreement with the recent results published by Hocquemiller et al. who used mouse cortical neurons obtained from E17 mouse embryos (Hocquemiller et al., 2010). This suggests that the presence of HEK293 did not significantly modify the growth parameters of cortical neurons.

In a second set of experiments, we analyzed the presence of Cntns at HEK293 cell surface and in culture supernatants. Immunofluorescence in permeabilized cells allows detecting both the surface and intracellular immunoreactivities. For each Cntn member, a proportional relationship could be observed between Cntn levels in supernatants and at the membrane of HEK293 cells. In addition, the level of each Cntn remained constant among the culture medium in independent experiments and between 48 and 72 hours of co-culture (data not shown). These observations strongly suggest a rapid turnover of Cntns and the lack of their accumulation in culture medium. For the purpose of this study, we considered cultivating neurons in the presence of transfected HEK293 cells instead of adding the HEK293 supernatants to the cultured neurons. Our aim was to maintain the neurons in their optimal growth conditions with neuronal medium and such a protocol had no apparent effect on the survival of HEK293 cells. In our cultured neurons, intracellular signaling pathways were successfully activated during shorter periods of exposition (<2 hours) in the presence of HEK293 cell supernatants containing soluble Cntns (unpublished data). In the absence of HEK293 cells, neurons do not secrete detectable amount of Cntns. Consequently, only a negligible amount of Cntns from neurons, which were not detectable by Western blotting, may have been released. This may also suggest that the density of anchored Cntns is much smaller in neurons than in transfected HEK293 cells. Anchored CAM-molecules, including the contactins, signal through heterophilic binding with distinct partners, and may also function as secreted ligands for receptor partners. For example, secreted forms, which remain folded and functional, have been described for the L1 cell adhesion glycoprotein (Gouveia et al., 2007). Such forms are able to contract both homophilic and heterophilic interactions with different partners. In the case of Cntn2 in rat (TAG-1), a membrane protein has been shown to be developmentally regulated in primary neuronal cell cultures, whereas a secreted protein persists over time (Karagogeos et al., 1991). Cntn2 in chicken (Axonin-1) has also been proposed to be released from dorsal root ganglia neurons (Lierheimer et al., 1997). Based on these observations, functional Cntn4, -5, and -6 are expected to be secreted after hydrolysis from the HEK293 cell surface. In our experiments, levels of Cntns in supernatants seemed to reach concentrations that have been shown to be high enough to enhance neurite outgrowth (Yoshihara et al., 1995; Sakurai et al.,

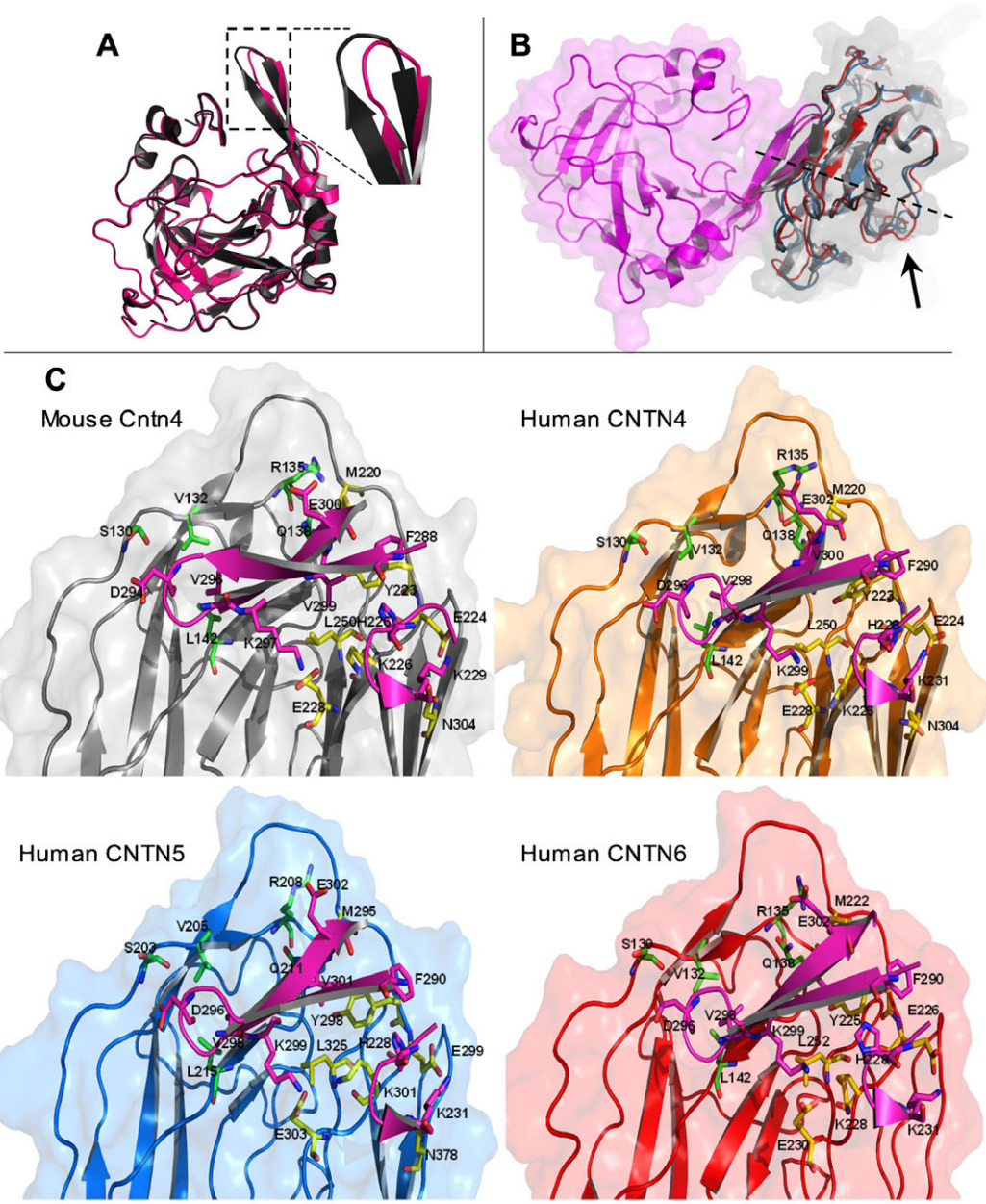

Fig. 6. Zoom magnification of the binding interfaces of the Ig-like domains of human CNTN4, -5 and -6 with the human PTPRG^{CA}. (**A**) Overlay of the carbonic anhydrase (CA) domain of mouse Ptprg with a model of the CA of human PTPRG obtained from the reference sequence of the mouse Ptprg with a specific focus on the β-hairpin (inset). Structural images were generated using PyMOL (http://www.pymol.org). (**B**) Alignment of the β-sheet structures within the complex between human CNTN$^{Ig1–4}$ and PTPRG^{CA} symbolized with the dotted line. Arrow indicates the close vicinity of the Ω loop. (**C**) Comparative surface representations of the four Ig-like domains of human CNTN4, -5, and -6 with binding of PTPRG. The same orientations are represented. Residues are shown as balls and sticks. Residues from CNTN^{Ig2}, CNTN^{Ig3} and PTPRG^{CA} are in green, yellow, and magenta, respectively, as presented in Bouyain and Watkins for mouse Cntn4 (Bouyain and Watkins, 2010a). Cntn4 is in gray, CNTN4 in yellow, CNTN5 in blue, and CNTN6 in red. Structural images were generated using PyMOL (http://www.pymol.org).

1997; Lee et al., 2000; Ogawa et al., 2001). As expected, the levels of secreted Cntns could be related to the number of HEK cells. At culture stages, prior to 8 days (8 DIV), the contacts between neuronal cells were not predominant suggesting that the effects were due to the Cntns secreted by HEK293 cells. This does not depend on surrounding neurons, which, as discussed above, do not secrete detectable levels of Cntns. These contacts may also depend on cell densities. Higher numbers of neurons could increase the number of contacts that could be sporadically observed in our co-culture. Moreover, we could not clearly detect the existence of true contacts between HEK cells and neuronal dendrites with the presence of punctae as putative synaptic

Table 1. Predicted parameters of interfaces between human CNTN$^{Ig1–4}$ and PTPRG^{CA}.

	Surface (Å)	delta G (kcal/mol)	H bonds	Salt bridges
Human [CNTN4_3KLD]	828	−7.1	3	4
Complex minimization	845	−5.5	10	13
Human [CNTN5_3KLD]	780	−9.6	7	5
Complex minimization	864	−9.0	8	5
Human [CNTN6_3KLD]	854	−9.0	8	5
Complex minimization	864	−3.6	15	9

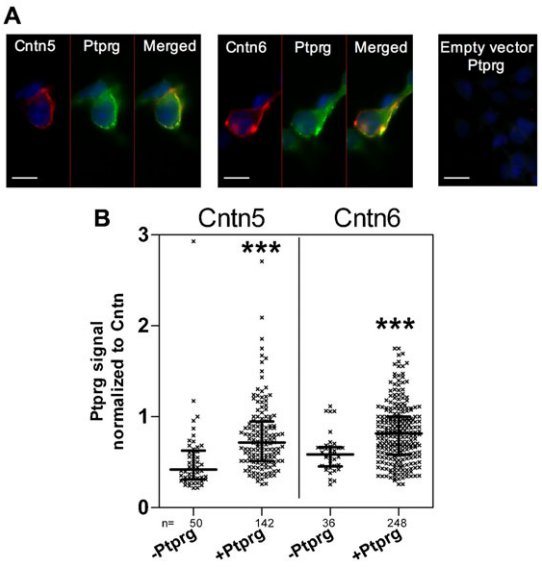

Fig. 7. Binding of Ptprg to HEK293 cells expressing the rat Cntn5 or Cntn6. HEK293 cells were transfected either with *Cntn5* or *Cntn6* cDNAs. Two days post-transfection, cells were incubated with Ptprg–Fc according to the protocol described in Materials and Methods. (**A**) In left and middle panels, red signals correspond to Cntn5 and -6, expressed at cell membranes. For Ptprg, positive labeling appears as lines of dots (green). Scale bars=20 µm. Right panel represents labeling in the absence of Cntn (empty vector) indicating no significant background in the absence of Ptprg binding. Note that the lines of dots are no longer visible. Scale bar=40 µm. (**B**) Semi-quantification of fluorescent signals in the absence and in the presence of Ptprg. Binding signals were normalized to Cntn fluorescence for each cell. Numbers of neurons analyzed are indicated in the graphs. Statistical analysis was performed using a Student's *t*-test. ***$P<0.001$.

boutons between cell types (neuron–neuron and neuron–glia/HEK293 cell).

We analyzed the effects of Cntn4, -5 and -6 and observed a significant increasing effect on neurite elongation and branching, as compared to conditions without Cntn. Our data are in agreement with previous observations showing that both substrate-bound and soluble forms of recombinant proteins of Cntn6 have a neurite outgrowth promoting effect on cortical neurons (Lee et al., 2000). Cntn5 has also been shown to increase neurite outgrowth in cerebral cortical neurons, but not in hippocampal neurons (Ogawa et al., 2001). Recombinant Cntn4 has been reported to promote neurite outgrowth when used as a substrate for neurons *in vitro* (Yoshihara et al., 1995). By contrast, Cntn4 has been reported to either reduce or display no effect on the axonal outgrowth of RGC axons, based on growth-matrix composition in protein partners (i.e. APP, NgCAM) and concomitant interactions (Osterfield et al., 2008). The effects of Cntn4 and -6 on branching parameters have not been reported previously.

Our data show distinct increasing effects between Cntn4, -5 and -6 on neuritogenesis. The effects of Cntn4 and -6 were more pronounced on neurite elongation and that of Cntn5 on branching. Cntn4 and -6 led to an increase in length and in the number of segments for the first stages of growth (at 4 DIV), then in the number of roots (at 6 DIV). By contrast to Cntn6, Cntn4 did not promote neurite elongation and branching at later stages of growth. Cntn5 selectively increased the number of roots at early stages of growth and promoted more progressively their branching. Such differences between Cntns effects could be related to the differential brain expression of each member and/or distinct signaling mechanisms. More widespread distributions of Cntn4 and -6 in the brain have been reported previously (Kaneko-Goto et al., 2008; Lee et al., 2000). By contrast, Cntn5 is specifically expressed in the auditory pathway (Toyoshima et al., 2009a) presenting complex neuronal organizations and dendritic morphologies (Okoyama et al., 2006).

Cntn functions are mediated by heterophilic protein interactions but the precise molecular mechanisms involved in their effects on neurite outgrowth have not been identified yet. Given that the Cntns do not possess any transmembrane and/or cytoplasmic domains, their ability to modulate neurite outgrowth may be dependent on their extracellular domains and adhesive properties. It may also involve other molecules and receptors that can transduce signals to cytoplasm.

Among possible signaling partners, Cntns have been shown to interact with amyloid precursor protein (APP) (Osterfield et al., 2008; Shimoda et al., 2012), Notch (Cui et al., 2004), and other Ig-CAMs. For example, the neural close homolog of L1 (CHL1) can associate with Cntn6 and both molecules interact with the protein tyrosine phosphatase alpha (PTPα), to regulate apical dendrite orientation in the developing caudal cortex (Ye et al., 2008). Of particular interest is that the three Cntn4, -5 and -6 have been recently shown to selectively interact with the protein tyrosine phosphatase gamma (Ptprg) (Bouyain and Watkins, 2010a). Using Ptprg knockout-LacZ transgenic mice, the expression of Ptprg was observed in the developing and adult brains, and this was restricted to pyramidal neurons in the adult mouse (Lamprianou et al., 2006). With the production of anti-Ptprg monoclonal antibodies, the expression of Ptprg in mouse cortical and hippocampal neurons has recently been evidenced presynaptically (Y.S., unpublished data). One can reasonably assume that rat cortical and hippocampal neurons would also express this protein. PTPRG is thought to mediate important signaling events through its tyrosine-specific phosphatase activity (Paul and Lombroso, 2003). PTPRG is therefore expected to control tyrosine dephosphorylation by contactin members. Accordingly, PTPRG has been shown to inhibit NGF-mediated neurite outgrowth of PC12D cells (Shintani et al., 2001); however, its specific role in neuritogenesis has not yet been clearly established.

Molecular and crystal structure analyses revealed that the first four immunoglobulin domains of Cntn structures are folded in a specific horseshoe-like structure. The PTPRG binding sites are located in the CA domain of this protein and contact at the second and third immunoglobulin domains of mouse Cntn4 (Bouyain and Watkins, 2010a).

We hypothesized that the differential effects of Cntn4, -5 and -6 on neuritogenesis could be partly explained by distinct binding properties that these molecules may have on the hairpin loop of the extracellular PTPRG^{CA}. The crystal structures of chicken and human contactin 2 (TAG-1) have been analyzed (Freigang et al., 2000; Mörtl et al., 2007). By contrast, the X-ray structures of human CNTN4–6 have not been identified yet. Only the first four Ig-like domains of mouse Cntn4 have been registered in the Protein Data Bank. We therefore built a model of the Ig1–4 domains for each of the human CNTN4, -5 and -6. We then identified the residues present at the interfaces between the CNTN domains and human PTPRG^{CA}. We chose the human sequences rather than rat sequences for a possible extrapolation of our data to human physiopathology.

Our data clearly indicate that the entire structure of human CNTN4$^{Ig1–4}$ can be superimposed to the mouse Cntn4$^{Ig1–4}$ whereas the human CNTN5$^{Ig1–4}$ and -6$^{Ig1–4}$ could not be fully superimposed to mouse and human CNTN4. Indeed, an insertion of an Ω loop was observed located at the interface between the Ig2 and Ig3 domains of human CNTN5 and -6, and predicted to be flexible (supplementary material Movie 1). The strong stability of Ig2 and Ig3 domains of human CNTN4 has been related to cellular functions of this protein (Mikulska et al., 2011). Since these domains interact directly with PTPRG^{CA}, it is possible that the presence of a flexible Ω loop in human CNTN5 and -6 within Ig2 and Ig3 domains, even if located quite remote from the interaction site, could have a functional relevance through its connectivity with the β strands of Ig3. For example, this plasticity could slightly modulate the binding affinity of human CNTN5 and -6 for PTPRG and thus modify its intracellular phosphatase activity. The residues that participate in the interactions between human PTPRG^{CA} and each human CNTN were found to be identical, and they were also identical to residues participating in the interaction between the murine Ptprg^{CA} and Cntn4$^{Ig1–4}$. We then measured the binding of Ptprg–Fc to rat Cntn5 and -6, when overexpressed by HEK293 cells. We did not find any significant modification in the intensity of Ptprg binding between the two Cntns. Our data strongly suggest that the differences in neurite outgrowth properties of Cntns that we observed in this study are not the consequence of molecular changes at Ptprg–Cntn interfaces. For Cntn5 and -6, they do not seem to result from changes in PTPRG binding capacities either. The mechanisms by which CNTN and PTPRG mediate their effects, locally or not, at cell membranes are far from being understood. It has been proposed that CNTN could facilitate the formation of PTPRG dimers with a resulting inhibition of its phosphatase activity (Bouyain and Watkins, 2010b). Alternatively, PTPRG and CNTN could function independently from phosphatase activity and rather promote the scaffolding of molecular signaling complexes (Bouyain and Watkins, 2010b). Such complexes could involve different partners among the CNTN members. In addition, the intracellular signaling pathways that are known to modulate neurite outgrowth and morphology of neurons could also be differentially activated by the CNTN members, independently from PTPRG. Finally, it should be noted that PTPRG could signal in a bidirectional manner, involving both phosphatase and carbonic anhydrase enzymatic activities.

In conclusion, we have developed an automated quantitative analysis of neuronal development that allows a more rapid screening of morphological characteristics with a high degree of accuracy and reproducibility. This method is particularly useful for the mutational screening of Ig-CAM molecules in disease since it circumvents the time-consuming purification and testing of each single mutated molecule if a coating procedure on slide would be retained. Our quantitative analysis of neuron morphology may be used to study various factors that could influence the development and functions of neurons that may be associated to brain disorders such as ASD. Our data show slight differences in the properties of Cntn4, -5 and -6 on neurite outgrowth that do not appear to be related to PTPRG. CNTN signaling is considered to be a very complex and cell-specific process. The identification of CNTN4, -5 and -6 protein networks, which may involve PTPRG, would be necessary to better understand their respective roles during neuritogenesis and brain wiring.

Materials and Methods

Animals

Pregnant Sprague-Dawley rats were obtained from Charles River Laboratories (L'Arbresle, France). Animals were housed in individual cages from weaning under a 12-hour light–dark cycle and controlled temperature (21℃) with water and food *ad libitum*. Adequate measures were taken to minimize pain or discomfort and experiments were carried out following the guidelines of the European Communities Council (86/609/EEC).

Cell culture procedures

HEK293 cells

HEK293 cells were cultured in Minimum Essential Medium (MEM) containing 100 units/ml penicillin, 100 µg/ml streptomycin, 2 mM glutamine (Invitrogen™, Life technologies SAS, Saint-Aubin, France) and 10% fetal calf serum (ref. CVFSVF00-01, Eurobio, Courtaboeuf, France) in a 5% CO_2 incubator at 37℃. Cells were grown in 100 mm Petri dishes. The day before transfection, cells were trypsinized, suspended in fresh medium and plated in 6-well plates containing glass coverslips. Coverslips were previously coated with 0.1 mg/ml of poly-L-Lysine (ref. P6282, Sigma–Aldrich Chimie, Saint-Quentin Fallavier, France). Cells were transfected either with rat Cntn4, Cntn5 or with Cntn6 cDNA sequences cloned in pcDNA3.1 vector (GenBank accession numbers for rat Cntn4, Cntn5 and Cntn6 are U35371, D87212 and D87248, respectively) using the jet PRIME® kit and according to the manufacturer's protocol (ref. POL114-15 Polyplus-transfection™ SA, Illkirch, France). At the end of transfection, 2–3×10^5 HEK293 cells per confluent 35 mm well were obtained. For co-culture assays and 24 hours post-transfection, cells were collected with neuronal culture medium containing 2 µM of Arabinofuranosylcytosine (Ara-C) (ref. C6645, Sigma–Aldrich, Chimie) kept warmed at 37℃. 2.5×10^5 HEK293 cells per ml of neuronal culture medium were seeded at the top of the neurons in culture (see below). For kinetics, HEK293 cells and neuronal cells were co-cultured for 48–72 hours before the fixation of cells (see below).

Primary rat cortical neurons

Primary rat cortical neurons enriched in hippocampal cells were prepared from newborn (P0–P1) Sprague-Dawley rats. Cortical and hippocampal tissues were dissected in HBSS/20 mM Hepes medium (ref. 14180-046 and 15630-049, Life technologies SAS). Tissues were then minced gently, digested with sterile papain (20 U/mL) (ref. LS003126, Worthington Biochemical Corporation, Lakewood, USA) in HBSS/Hepes for 10 minutes at 37℃, rinsed three times with HBSS/Hepes and then triturated in the presence of 1 mg/ml of DNase I for 5 minutes. After decantation, supernatants with dissociated neuronal cells were collected and diluted in Neurobasal medium® (ref. 21103-049, Life technologies SAS) supplemented with 1× B27®-supplement (Gibco®-Life Technologies SAS, France), L-glutamine (2 mM) and penicillin/streptomycin. Cells were counted using the Countess® automated cell-counter (Invitrogen™, Life technologies SAS, France) and plated at a density of 4×10^5 cells per mL onto poly-ornithine-coated (40 µg/mL; ref. P8638, Sigma–Aldrich Chimie) coverslips in 6-well plates. After 4 hours, the culture medium was replaced with fresh medium. Neurons were cultured for 2, 4 or 5–6 days before adding HEK293 cells.

Immunofluorescence

Immunofluorescence labeling on HEK293 cells was performed either in non-permeabilized or permeabilized conditions, in 6-well plates, 24 to 48 hours after transfection. Cells were fixed in the presence of 4% paraformaldehyde for 10 minutes at room temperature (RT) and washed 3 times in PBS. Cells were either directly saturated for 30 minutes in PBS containing 10% horse serum (ref. 16050-130, Life Technologies SAS), or permeabilized for 5 minutes in PBS/0.1% Triton then saturated as above. They were washed 3 times in PBS and incubated with the appropriate anti-Cntn primary antibody in PBS/0.1% Triton/2% horse serum for 2 hours at RT. Cells were washed 3 times in PBS and incubated with a fluorescent secondary antibody in PBS/0.1% Triton/2% horse serum for 1 hour at RT, and then washed again 3 times. Mouse anti-rat NB2 (3G12) and anti-rat NB3 (2F7) monoclonal antibodies amplified in ascites were used, at a dilution of 1/500 (Toyoshima et al., 2009b; Sakurai et al., 2009). These antibodies give a clear single band at approx. 130 kDa. The anti-Cntn4 antibody was purchased from R&D systems (AF2205, R&D Systems Inc., Minneapolis, USA) and used at a dilution of 1/200. For Cntn5 and Cntn6, the secondary antibody was an Alexa Fluor® 594 Goat Anti-Mouse IgG (H^+L) used at a dilution of 1/200 (A11005, Molecular Probes®, Life Technologies). For Cntn4, the secondary antibody was an Alexa Fluor® 488 Donkey Anti-Goat IgG (H^+L) used at a dilution of 1/200 (A11055, Molecular Probes®, Life Technologies). Cells were washed 3 times in PBS and rinsed once in milliQ water. Semi-quantitative analysis of fluorescence in permeabilized HEK293 cells was performed using Image J software. The relative cell surface expression of Cntn4, -5 and -6 was analyzed by measuring the pixel intensities of images from a confocal-like microscopy technique. The relative cell surface expression of Cntn4, -5 and -6 was analyzed by measuring the pixel intensities of images from a confocal-like microscopy technique. Immunofluorescence labeling on co-cultures was performed in

permeabilized conditions. Cells were fixed in the presence of 4% paraformaldehyde for 10 minutes at RT and washed 3 times in PBS, permeabilized and saturated in PBS/0.05% Triton/10% horse serum for 1 hour at RT under agitation. Antibody incubation was then performed in drops, with the primary monoclonal mouse anti-MAP2 antibody (ref. MAB3418, Millipore®, France) at a dilution of 1/500 in PBS/0.5% Tween 20/4% horse serum, overnight at 4℃. The day after, coverslips were washed 3 times in PBS/0.5% Tween 20, then incubated with the secondary antibody Alexa Fluor® 594 Goat Anti-Mouse IgG (H+L) (A11005, Molecular Probes, Life Technologies) at a dilution of 1/200 in PBS/0.5% Tween 20, for 45 minutes at RT. Cells were washed 3 times in PBS and rinsed once in milliQ water. Coverslips were then mounted on glass slides with ProLong Gold antifade reagent with DAPI (Invitrogen™, Life technologies SAS, France).

Western blot

To evaluate the presence of soluble/secreted Cntns in culture, aliquots of culture supernatants were collected and loaded on a 7% Tris-Acetate NuPage® Novex® Mini Gel (ref. EA0355BOX, Life technologies SAS) under reducing conditions according to the manufacturer's protocol. After electrophoresis, gels were transferred onto a PVDF membrane using the iBlot® 7-minute Western Blotting System (Life technologies SAS). Blots were saturated in PBS containing 0.5% milk powder, 1% BSA and 0.05% Tween 20, for 1 hour at RT. Blots were then incubated overnight at 4℃ in saturation buffer, with the primary antibody: anti-Cntn4 (ref. AF2205, dilution 1/250; R&D Systems, Inc., Minneapolis, USA), anti-Cntn5 (3G12, dilution 1/1000) or anti-Cntn6 (2F7; dilution 1/2000). After 3 washes in PBS/0.05% Tween 20 (PBS-T), blots were incubated for 1 hour at RT in the presence of adequate polyclonal anti-Ig HRP (Sigma) in PBS-T. After 3 washes, the respective Cntn bands were revealed by the ECL^{+} procedure (Amersham Biosciences, Orsay, France) as described by the supplier. Autoradiography was performed using BioMax MR Films and quantification of the bands by scanning densitometry. For whole-cell extract preparations, neurons or HEK293 cells were rinsed with ice-cold PBS, resuspended in lysis buffer (1 ml per 10^7 cells) containing 100 mM NaCl, 5 mM EDTA, 20 mM HEPES, 1% nonidet® P40, and a cocktail of protease inhibitors (ref. 11 873 580 001, Roche Diagnostics, Mannheim, Germany). After cell scraping, cell suspensions were transferred in microfuge tubes, maintained under constant agitation for at least 30 minutes at 4℃, and then centrifuged for 30 minutes at 10,000 rpm. Pellets were discarded, protein concentrations were measured in supernatants, and aliquots were submitted to gel electrophoresis as described above.

Image acquisition, processing and statistical analysis

Fluorescence images were acquired with an inverted microscope Axio Observer.Z1 (Carl Zeiss, Le Pecq, France) equipped with an AxioCam MR3 camera. For neurite detection, ten to fifteen mosaic images were acquired for each condition per experiment with a LD Plan-neofluar 20× objective and a 64HE mPlum reflector (Alexa 594 channel). Total image width and height were of 4041 and 3025 pixels, respectively. Each pixel represented 16 bit gray levels. Quantitative image analysis was performed using the Acapella image analysis, version 2.3 software (PerkinElmer, Inc.). A specific script for automated detection of neurons and analysis of their morphology was used. The same threshold parameters were applied in all conditions. Measured parameters extracted from specific module "neurite detection" include the length of the longest neurite per neuron, number of roots and total number of segments. Neurons without neurites were excluded from the analysis. Individual tracing of neurite extension was possible over all co-culture periods. Statistical analysis was performed using the Student's *t*-test and GraphPad Prism version 4 software (GraphPad, San Diego, California, USA).

Cell surface binding assay

Ptprg–Fc was constructed as a fusion protein of the extracellular domain (amino acids 1–172) of the mouse Ptprg and the Fc portion of human IgG, therefore lacking the intracellular phosphatase domain (mouse and rat Ptprg share 99.6% homology with identical contact residues with Cntn). Binding experiments were performed basically as described previously (Shimoda et al., 2012). In brief, HEK293 cells plated on glass coverslips were transfected with the *Cntn* plasmid using jetPRIME® kit, according to the manufacturer's protocol (polyplus-transfection SA, Illkirch, France). After 48 hours, the cells were fixed with 4% paraformaldehyde for 15 minutes at RT and washed 3 times with PBS. After washing, the cells were incubated with the Ptprg–Fc fusion protein (5 µg/ml) in PBS containing 10% normal goat serum and 0.5% BSA for 1 hour at RT. After washing with PBS 5 times, cells were incubated with Alexa Fluor 488-conjugated anti-human IgG (1:3000) for 1 hour at RT. After washing with PBS 5 times, cells were incubated with the 3G12 anti-Cntn5 antibody (1/500) or the 2F7 anti-Cntn6 antibody (1/500) for 1 hour at RT (Sakurai et al., 2009; Toyoshima et al., 2009a; Sakurai et al., 2010). After washing with PBS 5 times, the cells were incubated with an Alexa Fluor 594-conjugated anti-mouse IgG (1:200) for 1 hour at RT. After five washes with PBS, coverslips were mounted on glass slides. Fluorescent signals were quantified using a specific plugin of the Icy software (de Chaumont et al., 2012) (http://icy.bioimageanalysis.org). The plugin was based on wavelets detection to visualize the red fluorescence and provide the mean for the red and green fluorescent signals (Olivo-Marin, 2002). The Ptprg–Fc signals were normalized to the level of Cntn fluorescence at cell membrane. The plug-in is available on line (http://icy.bioimageanalysis.org/plugin/Ligand-Receptor_ratio_quantifier).

Homology modeling

The FASTA sequences of human $CNTN4^{Ig1–4}$, $CNTN5^{Ig1–4}$, $CNTN6^{Ig1–4}$ were retrieved from the UniProtKB server at (http://www.uniprot.org/uniprot) and 2D-aligned with the homologous mouse $Cntn4^{Ig1–4}$ as reference sequence (3KLD.fasta retrieved from the solved structure at http://www.rcsb.org/pdb/home/home.do) using ClustalW (http://www.ebi.ac.uk/Tools/msa/clustalw2). They were then 3D-aligned using Espript (http://espript.ibcp.fr/ESPript/ESPript) to include the mouse $Cntn4^{Ig1–4}$ secondary structure from the PDB entry 3KLD (Gouet et al., 1999; Bouyain and Watkins, 2010a). Human $CNTN4^{Ig1–4}$, $CNTN5^{Ig1–4}$, $CNTN6^{Ig1–4}$ were homology-modeled by computing both the alignment and the solved X-ray structure of the mouse $Cntn4^{Ig1–4}$ used as 3D template (Protein Data Bank ID: 3KLD). For each CNTN, 50 models were generated using the model-building software Modeller (mod9v7), to satisfy the spatial restraints issued from the alignment with the target protein (Eswar et al., 2006). Models with the lowest score function values and best stereochemistry and checked by Molprobity (http://molprobity.biochem.duke.edu) (Chen et al., 2010) were then subjected to subsequent refinement by energy minimization using CHARMM implemented in Discovery Studio 2.5 (DS2.5; Accelrys, Inc.) (Brooks et al., 2009). Similarly, the human $PTPRG^{CA}$ was homology-modeled using the mouse $Ptprg^{CA}$ as reference sequence for alignment and 3D template (from the 3D the complex of mouse $Cntn4^{Ig1–4}$/mouse $Ptprg^{CA}$). 50 models were generated; one was selected from its score function before being minimized using CHARMM forcefield. After optimization, each resulting model, CNTN4, -5 and $-6^{Ig1–4}$ or PTPRG was visually inspected with PyMOL and superimposed to the mouse $Cntn4^{Ig1–4}$–$Ptprg^{CA}$ complex template. Models of each complex between human CNTN4, -5 and -6 and human $PTPRG^{CA}$ were then optimized with an energy minimization where the backbone was kept fixed for the two proteins of the complex. Characteristics of the interface between each human CNTN and human PTPRG (surface size, residues, hydrogen bonds, salt bridges, energy parameters) were determined using the PISA server (http://www.ebi.ac.uk/msd-srv/prot_int/pistart.html).

Acknowledgements

This work was supported by the Institut Pasteur, INSERM, APHP, ANR (ANR-08-MNPS-037-01-SynGen), Neuron-ERANET (EUHF-AUTISM), Fondation Orange, Fondation pour la Recherche Médicale, RTRS Santé Mentale (Fondation FondaMental) and Fondation Bettencourt Schueller. O.M. is supported by an undergraduate fellowship from the Neuropole de recherche francilien (NeRF). We are grateful to Nathalie Lemière for her technical assistance.

Competing Interests

The authors have no competing interests to declare.

References

Alarcón, M., Abrahams, B. S., Stone, J. L., Duvall, J. A., Perederiy, J. V., Bomar, J. M., Sebat, J., Wigler, M., Martin, C. L., Ledbetter, D. H. et al. (2008). Linkage, association, and gene-expression analyses identify *CNTNAP2* as an autism-susceptibility gene. *Am. J. Hum. Genet.* **82**, 150-159.

Bakkaloglu, B., O'Roak, B. J., Louvi, A., Gupta, A. R., Abelson, J. F., Morgan, T. M., Chawarska, K., Klin, A., Ercan-Sencicek, A. G., Stillman, A. A. et al. (2008). Molecular cytogenetic analysis and resequencing of *Contactin Associated Protein-Like 2* in autism spectrum disorders. *Am. J. Hum. Genet.* **82**, 165-173.

Belmonte, M. K. and Bourgeron, T. (2006). Fragile X syndrome and autism at the intersection of genetic and neural networks. *Nat. Neurosci.* **9**, 1221-1225.

Bouyain, S. and Watkins, D. J. (2010a). The protein tyrosine phosphatases PTPRZ and PTPRG bind to distinct members of the contactin family of neural recognition molecules. *Proc. Natl. Acad. Sci. USA* **107**, 2443-2448.

Bouyain, S. and Watkins, D. J. (2010b). Identification of tyrosine phosphatase ligands for contactin cell adhesion molecules. *Commun. Integr. Biol.* **3**, 284-286.

Brooks, B. R., Brooks, C. L., 3rd, Mackerell, A. D., Jr, Nilsson, L., Petrella, R. J., Roux, B., Won, Y., Archontis, G., Bartels, C., Boresch, S. et al. (2009). CHARMM: the biomolecular simulation program. *J. Comput. Chem.* **30**, 1545-1614.

Burbach, J. P. and van der Zwaag, B. (2009). Contact in the genetics of autism and schizophrenia. *Trends Neurosci.* **32**, 69-72.

Chen, V. B., Arendall, W. B., 3rd, Headd, J. J., Keedy, D. A., Immormino, R. M., Kapral, G. J., Murray, L. W., Richardson, J. S. and Richardson, D. C. (2010). *MolProbity*: all-atom structure validation for macromolecular crystallography. *Acta Crystallogr. D Biol. Crystallogr.* **66**, 12-21.

Cottrell, C. E., Bir, N., Varga, E., Alvarez, C. E., Bouyain, S., Zernzach, R., Thrush, D. L., Evans, J., Trimarchi, M., Butter, E. M. et al. (2011). Contactin 4 as an autism susceptibility locus. *Autism Res.* **4**, 189-199.

Cui, X. Y., Hu, Q. D., Tekaya, M., Shimoda, Y., Ang, B. T., Nie, D. Y., Sun, L., Hu, W. P., Karsak, M., Duka, T. et al. (2004). NB-3/Notch1 pathway via Deltex1 promotes neural progenitor cell differentiation into oligodendrocytes. *J. Biol. Chem.* **279**, 25858-25865.

de Chaumont, F., Dallongeville, S., Chenouard, N., Hervé, N., Pop, S., Provoost, T., Meas-Yedid, V., Pankajakshan, P., Lecomte, T., Le Montagner, Y. et al. (2012). Icy: an open bioimage informatics platform for extended reproducible research. *Nat. Methods* **9**, 690-696.

Ensslen-Craig, S. E. and Brady-Kalnay, S. M. (2004). Receptor protein tyrosine phosphatases regulate neural development and axon guidance. *Dev. Biol.* **275**, 12-22.

Eswar, N., Webb, B., Marti-Renom, M. A., Madhusudhan, M. S., Eramian, D., Shen, M.-Y., Pieper, U. and Sali, A. (2006). Comparative protein structure modeling using MODELLER. *Curr. Protoc. Bioinformatics* **15**, 5.6.1-5.6.30.

Freigang, J., Proba, K., Leder, L., Diederichs, K., Sonderegger, P. and Welte, W. (2000). The crystal structure of the ligand binding module of axonin-1/TAG-1 suggests a zipper mechanism for neural cell adhesion. *Cell* **101**, 425-433.

Geschwind, D. H. and Levitt, P. (2007). Autism spectrum disorders: developmental disconnection syndromes. *Curr. Opin. Neurobiol.* **17**, 103-111.

Glessner, J. T., Wang, K., Cai, G., Korvatska, O., Kim, C. E., Wood, S., Zhang, H., Estes, A., Brune, C. W., Bradfield, J. P. et al. (2009). Autism genome-wide copy number variation reveals ubiquitin and neuronal genes. *Nature* **459**, 569-573.

Gollan, L., Salomon, D., Salzer, J. L. and Peles, E. (2003). Caspr regulates the processing of contactin and inhibits its binding to neurofascin. *J. Cell Biol.* **163**, 1213-1218.

Gouet, P., Courcelle, E., Stuart, D. I. and Métoz, F. (1999). ESPript: analysis of multiple sequence alignments in PostScript. *Bioinformatics* **15**, 305-308.

Gouveia, R. M., Morais, V. A., Peixoto, C., Sousa, M., Regalla, M., Alves, P. M. and Costa, J. (2007). Production and purification of functional truncated soluble forms of human recombinant L1 cell adhesion glycoprotein from *Spodoptera frugiperda* Sf9 cells. *Protein Expr. Purif.* **52**, 182-193.

Hocquemiller, M., Vitry, S., Bigou, S., Bruyère, J., Ausseil, J. and Heard, J. M. (2010). GAP43 overexpression and enhanced neurite outgrowth in mucopolysaccharidosis type IIIB cortical neuron cultures. *J. Neurosci. Res.* **88**, 202-213.

Huang, Z., Yu, Y., Shimoda, Y., Watanabe, K. and Liu, Y. (2012). Loss of neural recognition molecule NB-3 delays the normal projection and terminal branching of developing corticospinal tract axons in the mouse. *J. Comp. Neurol.* **520**, 1227-1245.

Kaneko-Goto, T., Yoshihara, S., Miyazaki, H. and Yoshihara, Y. (2008). BIG-2 mediates olfactory axon convergence to target glomeruli. *Neuron* **57**, 834-846.

Karagogeos, D., Morton, S. B., Casano, F., Dodd, J. and Jessell, T. M. (1991). Developmental expression of the axonal glycoprotein TAG-1: differential regulation by central and peripheral neurons *in vitro*. *Development* **112**, 51-67.

Labasque, M. and Faivre-Sarrailh, C. (2010). GPI-anchored proteins at the node of Ranvier. *FEBS Lett.* **584**, 1787-1792.

Lamprianou, S., Vacaresse, N., Suzuki, Y., Meziane, H., Buxbaum, J. D., Schlessinger, J. and Harroch, S. (2006). Receptor protein tyrosine phosphatase γ is a marker for pyramidal cells and sensory neurons in the nervous system and is not necessary for normal development. *Mol. Cell. Biol.* **26**, 5106-5119.

Lee, S., Takeda, Y., Kawano, H., Hosoya, H., Nomoto, M., Fujimoto, D., Takahashi, N. and Watanabe, K. (2000). Expression and regulation of a gene encoding neural recognition molecule NB-3 of the contactin/F3 subgroup in mouse brain. *Gene* **245**, 253-266.

Lierheimer, R., Kunz, B., Vogt, L., Savoca, R., Brodbeck, U. and Sonderegger, P. (1997). The neuronal cell-adhesion molecule axonin-1 is specifically released by an endogenous glycosylphosphatidylinositol-specific phospholipase. *Eur. J. Biochem.* **243**, 502-510.

Mikulska, K., Pepłowski, L. and Nowak, W. (2011). Nanomechanics of Ig-like domains of human contactin (BIG-2). *J. Mol. Model.* **17**, 2313-2323.

Morrow, E. M., Yoo, S. Y., Flavell, S. W., Kim, T. K., Lin, Y., Hill, R. S., Mukaddes, N. M., Balkhy, S., Gascon, G., Hashmi, A. et al. (2008). Identifying autism loci and genes by tracing recent shared ancestry. *Science* **321**, 218-223.

Mörtl, M., Sonderegger, P., Diederichs, K. and Welte, W. (2007). The crystal structure of the ligand-binding module of human TAG-1 suggests a new mode of homophilic interaction. *Protein Sci.* **16**, 2174-2183.

Murai, K. K., Misner, D. and Ranscht, B. (2002). Contactin supports synaptic plasticity associated with hippocampal long-term depression but not potentiation. *Curr. Biol.* **12**, 181-190.

Ogawa, J., Kaneko, H., Masuda, T., Nagata, S., Hosoya, H. and Watanabe, K. (1996). Novel neural adhesion molecules in the Contactin/F3 subgroup of the immunoglobulin superfamily: isolation and characterization of cDNAs from rat brain. *Neurosci. Lett.* **218**, 173-176.

Ogawa, J., Lee, S., Itoh, K., Nagata, S., Machida, T., Takeda, Y. and Watanabe, K. (2001). Neural recognition molecule NB-2 of the contactin/F3 subgroup in rat: specificity in neurite outgrowth-promoting activity and restricted expression in the brain regions. *J. Neurosci. Res.* **65**, 100-110.

Okoyama, S., Ohbayashi, M., Ito, M. and Harada, S. (2006). Neuronal organization of the rat inferior colliculus participating in four major auditory pathways. *Hear. Res.* **218**, 72-80.

Olivo-Marin, J.-C. (2002). Extraction of spots in biological images using multiscale products. *Pattern Recognit.* **35**, 1989-1996.

Osterfield, M., Egelund, R., Young, L. M. and Flanagan, J. G. (2008). Interaction of amyloid precursor protein with contactins and NgCAM in the retinotectal system. *Development* **135**, 1189-1199.

Paul, S. and Lombroso, P. J. (2003). Receptor and nonreceptor protein tyrosine phosphatases in the nervous system. *Cell. Mol. Life Sci.* **60**, 2465-2482.

Peles, E., Nativ, M., Campbell, P. L., Sakurai, T., Martinez, R., Lev, S., Clary, D. O., Schilling, J., Barnea, G., Plowman, G. D. et al. (1995). The carbonic anhydrase domain of receptor tyrosine phosphatase β is a functional ligand for the axonal cell recognition molecule contactin. *Cell* **82**, 251-260.

Peñagarikano, O., Abrahams, B. S., Herman, E. I., Winden, K. D., Gdalyahu, A., Dong, H., Sonnenblick, L. I., Gruver, R., Almajano, J., Bragin, A. et al. (2011). Absence of CNTNAP2 leads to epilepsy, neuronal migration abnormalities, and core autism-related deficits. *Cell* **147**, 235-246.

Pierre, K., Dupouy, B., Allard, M., Poulain, D. A. and Theodosis, D. T. (2001). Mobilization of the cell adhesion glycoprotein F3/contactin to axonal surfaces is activity dependent. *Eur. J. Neurosci.* **14**, 645-656.

Roohi, J., Montagna, C., Tegay, D. H., Palmer, L. E., DeVincent, C., Pomeroy, J. C., Christian, S. L., Nowak, N. and Hatchwell, E. (2009). Disruption of contactin 4 in three subjects with autism spectrum disorder. *J. Med. Genet.* **46**, 176-182.

Rougon, G., Olive, S., Durbec, P., Faivre-Sarrailh, C. and Gennarini, G. (1994). Functional studies and cellular distribution of the F3 GPI-anchored adhesion molecule. *Braz. J. Med. Biol. Res.* **27**, 409-414.

Sakurai, T., Lustig, M., Nativ, M., Hemperly, J. J., Schlessinger, J., Peles, E. and Grumet, M. (1997). Induction of neurite outgrowth through contactin and Nr-CAM by extracellular regions of glial receptor tyrosine phosphatase β. *J. Cell Biol.* **136**, 907-918.

Sakurai, K., Toyoshima, M., Ueda, H., Matsubara, K., Takeda, Y., Karagogeos, D., Shimoda, Y. and Watanabe, K. (2009). Contribution of the neural cell recognition molecule NB-3 to synapse formation between parallel fibers and Purkinje cells in mouse. *Dev. Neurobiol.* **69**, 811-824.

Sakurai, K., Toyoshima, M., Takeda, Y., Shimoda, Y. and Watanabe, K. (2010). Synaptic formation in subsets of glutamatergic terminals in the mouse hippocampal formation is affected by a deficiency in the neural cell recognition molecule NB-3. *Neurosci. Lett.* **473**, 102-106.

Salzer, J. L., Brophy, P. J. and Peles, E. (2008). Molecular domains of myelinated axons in the peripheral nervous system. *Glia* **56**, 1532-1540.

Saus, E., Brunet, A., Armengol, L., Alonso, P., Crespo, J. M., Fernández-Aranda, F., Guitart, M., Martín-Santos, R., Menchón, J. M., Navinés, R. et al. (2010). Comprehensive copy number variant (CNV) analysis of neuronal pathways genes in psychiatric disorders identifies rare variants within patients. *J. Psychiatr. Res.* **44**, 971-978.

Sharom, F. J. and Lehto, M. T. (2002). Glycosylphosphatidylinositol-anchored proteins: structure, function, and cleavage by phosphatidylinositol-specific phospholipase C. *Biochem. Cell Biol.* **80**, 535-549.

Shimoda, Y. and Watanabe, K. (2009). Contactins: emerging key roles in the development and function of the nervous system. *Cell Adh. Migr.* **3**, 64-70.

Shimoda, Y., Koseki, F., Itoh, M., Toyoshima, M. and Watanabe, K. (2012). A cis-complex of NB-2/contactin-5 with amyloid precursor-like protein 1 is localized on the presynaptic membrane. *Neurosci. Lett.* **510**, 148-153.

Shintani, T., Maeda, N. and Noda, M. (2001). Receptor-like protein tyrosine phosphatase γ (RPTPγ), but not PTPζ/RPTPβ, inhibits nerve-growth-factor-induced neurite outgrowth in PC12D cells. *Dev. Neurosci.* **23**, 55-69.

Stoeckli, E. T. (2004). Ig superfamily cell adhesion molecules in the brain. *Handb. Exp. Pharmacol.* **165**, 373-401.

Stoeckli, E. T. (2010). Neural circuit formation in the cerebellum is controlled by cell adhesion molecules of the Contactin family. *Cell Adh. Migr.* **4**, 523-526.

Ting, A. E. and Pagano, R. E. (1991). Density-dependent inhibition of cell growth is correlated with the activity of a cell surface phosphatidylinositol-specific phospholipase C. *Eur. J. Cell Biol.* **56**, 401-406.

Toyoshima, M., Sakurai, K., Shimazaki, K., Takeda, Y., Nakamoto, M., Serizawa, S., Shimoda, Y. and Watanabe, K. (2009a). Preferential localization of neural cell recognition molecule NB-2 in developing glutamatergic neurons in the rat auditory brainstem. *J. Comp. Neurol.* **513**, 349-362.

Toyoshima, M., Sakurai, K., Shimazaki, K., Takeda, Y., Shimoda, Y. and Watanabe, K. (2009b). Deficiency of neural recognition molecule NB-2 affects the development of glutamatergic auditory pathways from the ventral cochlear nucleus to the superior olivary complex in mouse. *Dev. Biol.* **336**, 192-200.

Valtorta, F. and Leoni, C. (1999). Molecular mechanisms of neurite extension. *Philos. Trans. R. Soc. Lond. B Biol. Sci.* **354**, 387-394.

van Daalen, E., Kemner, C., Verbeek, N. E., van der Zwaag, B., Dijkhuizen, T., Rump, P., Houben, R., van 't Slot, R., de Jonge, M. V., Staal, W. G. et al. (2011). Social Responsiveness Scale-aided analysis of the clinical impact of copy number variations in autism. *Neurogenetics* **12**, 315-323.

Ye, H., Tan, Y. L., Ponniah, S., Takeda, Y., Wang, S. Q., Schachner, M., Watanabe, K., Pallen, C. J. and Xiao, Z. C. (2008). Neural recognition molecules CHL1 and NB-3 regulate apical dendrite orientation in the neocortex via PTPα. *EMBO J.* **27**, 188-200.

Ye, H., Zhao, T., Tan, Y. L., Liu, J., Pallen, C. J. and Xiao, Z. C. (2011). Receptor-like protein-tyrosine phosphatase α enhances cell surface expression of neural adhesion molecule NB-3. *J. Biol. Chem.* **286**, 26071-26080.

Yoshihara, Y., Kawasaki, M., Tamada, A., Nagata, S., Kagamiyama, H. and Mori, K. (1995). Overlapping and differential expression of BIG-2, BIG-1, TAG-1, and F3: four members of an axon-associated cell adhesion molecule subgroup of the immunoglobulin superfamily. *J. Neurobiol.* **28**, 51-69.

Zuko, A., Bouyain, S., van der Zwaag, B. and Burbach, J. P. (2011). Contactins: structural aspects in relation to developmental functions in brain disease. *Adv. Protein Chem. Struct. Biol.* **84**, 143-180.

Supplementary Material
Oriane Mercati et al. doi: 10.1242/bio.20133343

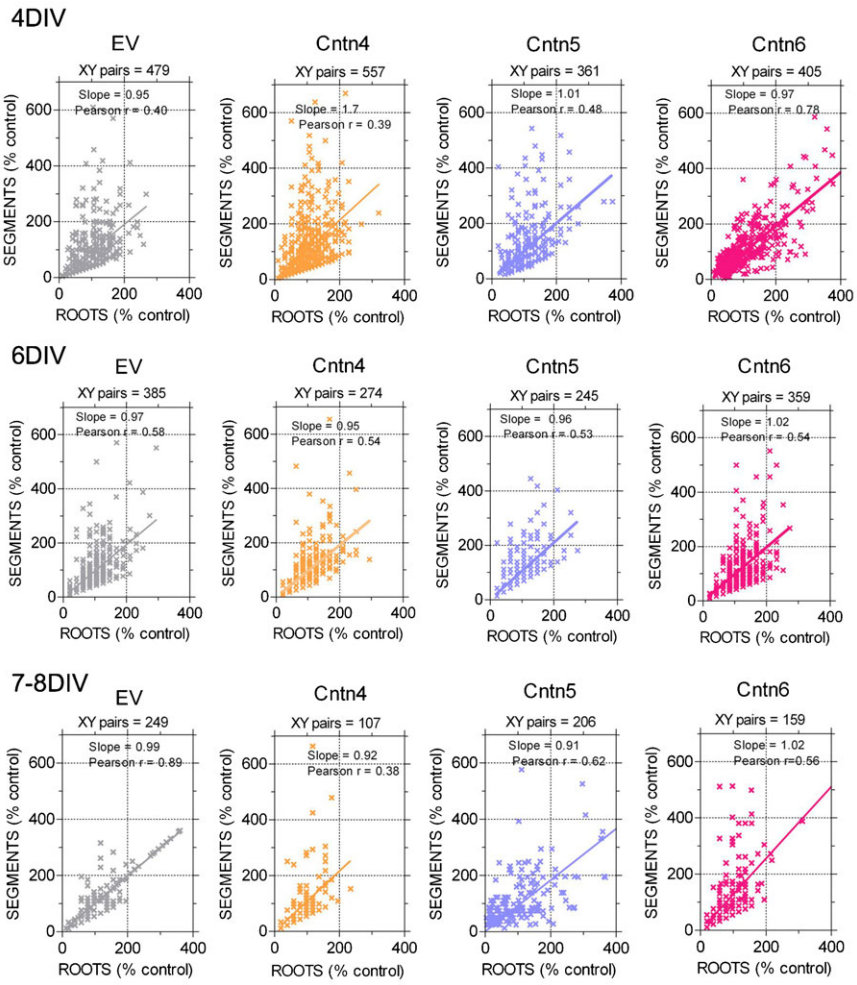

Fig. S1. Comparative effects of secreted Cntn4, -5, and -6 on arborization in rat cortical neurons in culture, at different time intervals. Cultures of rat cortical neurons were established from newborn rats (P0–P1) as described in Materials and Methods. Neurons were kept for up to 8 days in culture (DIV). The same densities of HEK293 cells were added 48–72 hours before the end of culture, in all conditions (see Materials and Methods). The length of the longest neurite per neuron, the total number of roots, and the segments were followed over time in all conditions. At the end of culture, neurons were fixed and immunostained with an anti-MAP2 antibody. Quantification was performed using Acapella software. Numbers of neurons analyzed are indicated in each graph. A two-dimensional representation showing the number of roots *versus* number of segments illustrates the evolution of neuronal trees over the different co-culture periods. Data are expressed as percent of control mean obtained in the absence of Cntn. Slope values and the Pearson's correlation coefficients are directly indicated in the graphs.

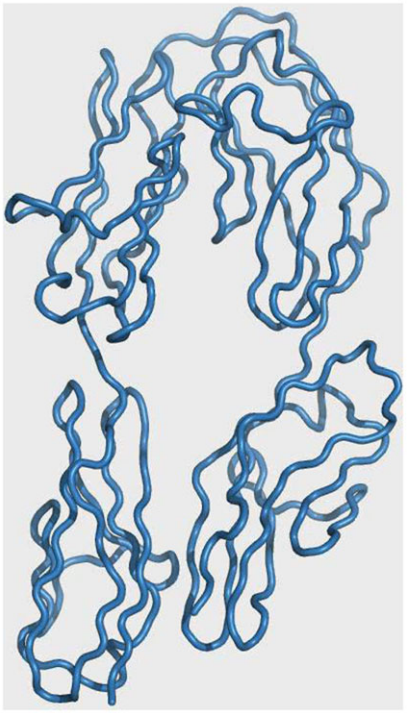

Movie 1. Flexible Ω loop in human CNTN5$^{Ig1–4}$. Three-dimensional structure of human CNTN5$^{Ig1–4}$ after homology modeling using the mouse Cntn4$^{Ig1–4}$ as a template (Bouyain and Watkins, 2010a). The flexible Ω loop in human CNTN5$^{Ig1–4}$ is located within Ig2 and Ig3 domains and can adopt distinct positions.